Eur. Phys. J. B **26**, 455–465 (2002)
DOI: 10.1140/epjb/e20020114

THE EUROPEAN PHYSICAL JOURNAL B
EDP Sciences

Overhauser shift of the electron spin-resonance line of Si:P at the metal-insulator transition: II. ^{29}Si contribution

U. Fasol[a] and E. Dormann

Physikalisches Institut, Universität Karlsruhe (TH), 76128 Karlsruhe, Germany

Received 8 November 2001

Abstract. The electron-spin resonance (ESR) line of delocalised electrons shifts upon saturation due to the hyperfine interaction with the dynamically polarized nuclear spins. The ^{29}Si part of the Overhauser shift of the ESR line of phosphorus doped silicon (Si:P) is separated in the concentration range 2.7 ... $7.3 \times 10^{18}/\mathrm{cm}^3$ covering the metal-insulator transition. The Overhauser shift profiles, recorded *versus* ^{29}Si nuclear magnetic resonance (NMR) frequency, are asymmetric. Their dependence on temperature and ESR saturation compares reasonably with simulations. Time and NMR frequency dependence of the dynamic nuclear polarization is studied in detail. No pronounced variation of the ^{29}Si Overhauser shift profiles with P concentration is observed, but the maximum value of the shift profile decreases with increasing P concentration. In contrast to standard ^{29}Si NMR results, these measurements reveal the behaviour of the ^{29}Si nuclei close to the P doping sites.

PACS. 76.70.-r Magnetic double resonances and cross effects – 71.30.+h Metal-insulator transitions and other electronic transitions

1 Introduction

Phosphorus atoms have one electron more than Si-atoms. These electrons are weakly bound in phosphorus doped silicon and their wave function is spread over several lattice constants. At P-concentrations higher than a critical concentration ($N_c = 3.52 \times 10^{18}/\mathrm{cm}^3$ [1]) the crystals become metallic. Below this critical concentration the crystals are semiconducting. The electronic wave function in the transition range can be probed by magnetic resonance techniques. The isotropic hyperfine interaction (Fermi contact interaction) is proportional to the electron density at the nucleus. The hyperfine interaction of the localized donor electron with the ^{29}Si ($I = 1/2$) nuclei, situated at different neighbouring lattice sites, was analysed by Feher [2] for a sample with $N = 5 \times 10^{16}/\mathrm{cm}^3$ ($\ll N_c$). He used the classical electron nuclear double resonance (ENDOR) technique for the measurements, and a wave function with a hydrogen-like envelope function for the analysis. For isolated donor electrons the electron spin resonance (ESR) line is split into two lines by the hyperfine interaction with the central ^{31}P-nucleus ($I = 1/2$). At P-concentration higher than about $1 \times 10^{18}/\mathrm{cm}^3$, which is still lower than N_c, the exchange interaction between nearest neighbour electron spins is so large, that most of the electron spins are not localized around one P-atom anymore. As a result in ESR experiments only one (exchange narrowed) line is observed. Since there are not as many nuclear spins parallel as antiparallel to the external field, the electron spins still experience an average non zero hyperfine field. But for Si:P at thermal equilibrium, at temperatures above 4 K, this field is at least seven orders of magnitude smaller than the external field for 10 GHz-ESR. Since the nuclear Zeeman interaction is about a factor of 2000 smaller than that of the electron spins, it should be easier to detect the relative shift of the nuclear magnetic resonance (NMR) line by the hyperfine interaction (Paramagnetic shift or Knight shift). But in the vicinity of N_c the ratio of P-atoms to Si-atoms is only about 1:14000. A standard NMR spectrum of ^{29}Si nuclear spins (natural abundance 4.7%, ^{28}Si and ^{30}Si have no nuclear spin) is dominated by the Si-bulk and the signal of the ^{29}Si neighbours to the P atom is wiped out. On the other hand the number of ^{31}P nuclear spins (natural abundance 100%) in the sample is very small and the ^{31}P NMR-signal hardly detectable.

A unique possibility to learn more about the hyperfine interaction and therefore about the donor electrons is to analyse the Overhauser shift of the ESR line. If the ESR transition is partly saturated, the nuclear spin polarization is strongly increased by the so called Overhauser effect [3]. At cw ESR experiments the frequency is kept constant, given by the cavity, and the external static magnetic field is swept. The enhanced hyperfine field by the increased nuclear spin polarization results in a shift of the ESR-line, the so called Overhauser shift. In Si:P the resulting shift is towards lower external field (due to a positive resulting hyperfine field) [4] and represents the integral over the effect by ^{29}Si and ^{31}P nuclear spins. In

[a] e-mail: ulli@piobelix.physik.uni-karlsruhe.de

order to separate the Overhauser shift caused by the Si nuclear spins from that caused by the P nuclear spins, it is necessary to destroy the polarization separately [5,6]. This is possible, because the NMR frequencies are different: $\nu_{\rm P}/\nu_{\rm Si} \approx 2$. Since the measurement is based on the ESR, the advantage of its better signal to noise ratio can be utilized. The hyperfine interaction at the P-atom, as well as that of those Si nuclear spins which are nearby the P-atoms, can be analysed. Thus, the local interaction at the donor site and its nearest neighbour sites can be studied. Applications of methods based on this principle to Si:P in the semiconducting region, with $N = 0.7N_c$ and $N = 0.85N_c$, were published previously [5,7,8].

For this work, samples with $N = 2.7$–$7.3 \times 10^{18}/\mathrm{cm}^3$ ($N = 0.77$–$2.07N_c$) have been measured at 5–11 K. In the following, the samples are labelled according to their P-concentration, *e.g.* N5.1.3 is sample number 3 of P-concentration $5.1 \times 10^{18}/\mathrm{cm}^3$. The results of the microwave conductivity, ESR g-factor, line-width and saturation behaviour, and the integral Overhauser shift of the ESR-line have been published earlier [4]. In this paper results of measurement and simulation of the contribution of the Si nuclear spins to the ESR-line Overhauser shift will be shown and analysed. The experimental details are given in Section 2 of the paper. In Section 3 the shift-profiles and their simulations are introduced, and the influence of ESR-saturation and temperature are described. Section 4 gives the results of the time dependent measurements, and in Section 5 the change of the shift profiles with P-concentration is presented and discussed. The analysis of the amplitude of the profiles (absolute shift values) is detailed in Section 6. A discussion and the conclusions are given in Sections 7 and 8, respectively.

2 Experimental details

Platelet-like flat samples of area $\approx$ 1.3–3.4 mm^2 and thickness 0.025–0.081 mm, *i.e.* less than the skin depth were prepared [4,9]. For the ESR-experiments an X-band Bruker ESP300E spectrometer with an ER4118 dielectric resonator and an Oxford instruments cryostat was used. A probehead was developped so that, in addition to the microwave field (9.8 GHz) for the electron spins, a radiofrequency power for the ^{29}Si-nuclear spins ($\approx$3 MHz) can be applied. Because the probehead with the sample and the RF-coil is inserted into the ESR-cavity, the loss of the quality factor had to be minimized. In the temperature region of 5–11 K the ER4118-cavity with the probehead has a quality factor of $Q \approx 12000$. With the Si:P samples the quality factor was between $Q \approx 9600 \pm 700$ (N2.7) and $Q \approx 5000 \pm 500$ (N7.3.1). The decrease of the quality factor with increasing P-concentration is caused by the increasing conductivity. The degree of saturation of the ESR-line was determined with the help of the ESR-line shape [4,9]. It is given below by the saturation factor:

$$s = \frac{S_0 - \langle S_z \rangle}{S_0} \qquad (1)$$

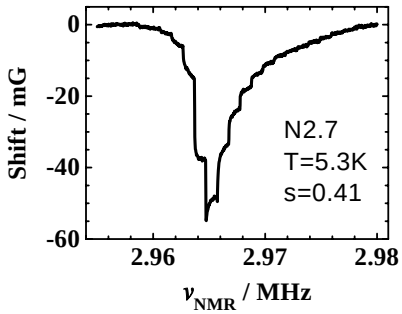

Fig. 1. A typical Si-Overhauser shift profile, measured with N2.7 at 5.3 K for step-like increasing NMR frequency. ($\nu_{ESR} =$ 9.8 GHz, $B_0 \approx 3.5$ kG.)

where S_0 is the average value of S_z at thermal equilibrium. At full saturation the two ESR energy levels have the same occupation and so $\langle S_z \rangle = 0$, $s = 1$. At thermal equilibrium $\langle S_z \rangle = S_0$ and therefore $s = 0$. For additional experimental details see [9].

2.1 Measurement of the profiles

As a first step, the ESR-line (derivative) at a constant microwave power (P_{ESR}) is recorded and the line position (B_0) is determined. For the measurement of the Overhauser shift profile, the external static magnetic field (B_{Mess}) is adjusted to this field ($B_{Mess} = B_0$) and held constant (field-frequency lock). The ESR signal amplitude at this field is then detected, while the radiofrequency is swept through the resonance of the ^{29}Si nuclear spins. If the RF-frequency reaches the resonance frequency of some of the Si nuclear spins, their polarization is reduced. As a result the ESR-line is partly shifted back ($B_0 \neq B_{Mess}$ anymore) and the ESR signal amplitude at B_{Mess} changes. Using the known shape of the "virgin" ESR line obtained in the first step, it is possible to calculate from the ESR-signal amplitude at each RF-frequency the corresponding back-shift of the ESR-line. Thus, the Overhauser shift profiles show at each RF-frequency the contribution to the Overhauser shift caused by the ^{29}Si resonating at this frequency. A typical example is shown in Figure 1. With this method it is possible to detect the distribution of the Overhauser shifts within the Si nuclear spins. The possible frequency steps of the RF-synthesizer are $\geq$1 kHz. The scanning rate was typically to 1 kHz/26s (see below). All shift values reported below for ^{29}Si are negative. This means, that the ESR line shifts to lower external field, if the corresponding ^{29}Si contribution is eliminated by NMR saturation. Thus, the dynamically polarized ^{29}Si nuclear spins must have a negative hyperfine field contribution to the ESR-field.

2.2 Time dependent measurement

For the time dependent measurement the ESR-signal amplitude was detected at locked magnetic field and constant RF-frequency. By switching on and off the RF-frequency

power and monitoring the time-dependence of the resulting signal, it is possible to determine the time constant of building up the nuclear spin polarization. For this measurement the signal was detected with a HP54520C oscilloscope. A relay controlled by a computer was used to switch on and off the RF-power and give the trigger to the oscilloscope.

3 The ^{29}Si-Overhauser shift profiles

3.1 A typical measured Si-profile

Figure 1 shows a typical Si-Overhauser shift profile for the sample with $N = 2.7 \times 10^{18}/\mathrm{cm}^3$ at 5.3 K and an ESR saturation factor of $s = 0.41$. The step like form is caused by the 1 kHz NMR-frequency steps. Since between two frequency steps the signal was detected at constant frequency, the form of the steps shows that there are fast and slow time dependent processes. (see Sect. 4 for a detailed discussion.)

The shape of the shift-profile is not symmetric (Fig. 1). It has a steep decrease at low frequencies and a slower increase at the high frequency side. The asymmetry is caused by a distribution between the Si-nuclear spins (Sect. 3.3).

In principle it is possible to build up an Overhauser enhanced nuclear spin polarization *via* both the anisotropic dipolar and the isotropic Fermi contact hyperfine interaction. The resulting polarization and therefore the Overhauser shift have opposite sign depending on the relative magnitudes of these two interactions. The sign of the shift in the profile of the Si nuclear spins (Fig. 1) shows that the Fermi contact interaction is the dominant interaction for the Si nuclear spins in Si:P. By the dynamically polarized ^{29}Si nuclear spins, a negative (hyperfine) field at the electron spins is created (that, if reduced by NMR, results in an ESR line shift to lower external field).

3.2 Influence of the radio-frequency power

If the radiofrequency power (P_{NMR}) for the nuclear spins is applied in addition to the microwave power (P_{ESR}) for the electron spins, two processes compete against each other: The nuclear spin polarization is enhanced *via* P_{ESR} and the resulting ESR line saturation, but the nuclear spin polarization is destroyed by P_{NMR} again. This means, that at constant P_{ESR} the magnitude of the Overhauser shift profile is expected to increase with increasing P_{NMR}. This behaviour is shown in Figure 2. At constant ESR-saturation ($s = 0.63$) several profiles have been measured at different P_{NMR}. The extremum of the shift-profiles increases with increasing P_{NMR}. Additionally, the profile broadens, and the steep decrease at lower frequencies is influenced stronger than the more flat part of the profile at higher frequencies. Thus the profile becomes more symmetric. A possible explanation is that the increasing P_{NMR} allows to reduce already the spin polarization of the off-resonant ^{29}Si nuclear spins by irradiation in the far wings of their

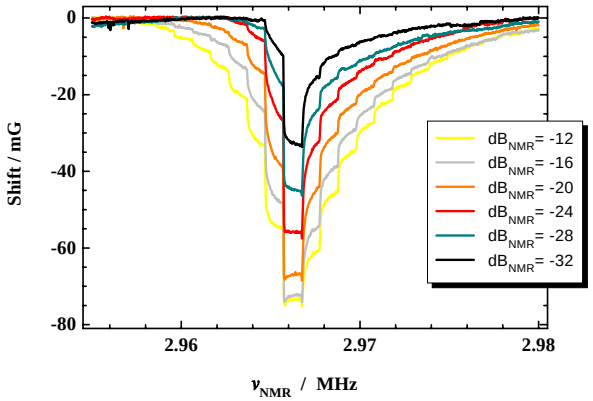

Fig. 2. Change of the measured shift-profile with increasing radiofrequency power (0dB$_{\mathrm{NMR}}$ corresponds to approximately 30 W). (N3.55, $T = 5.4$ K and $s = 0.63$).

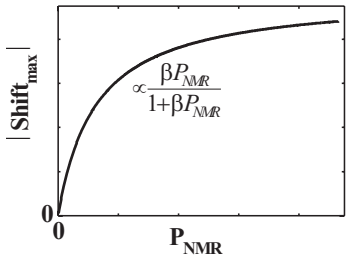

Fig. 3. Shift of the ESR-line for destroying partly the ^{29}Si part of the nuclear spin polarization *versus* the RF-/NMR-power.

respective resonance lines. Superimposed on this process is line broadening of the NMR spectrum by increasing NMR saturation with increasing P_{NMR}.

The increase of the extremum of the profiles with increasing P_{NMR} shows a saturation-like behaviour (Fig. 2). If the polarization of the nuclear spins is reduced to zero, which means as many nuclear spins are parallel as antiparallel to the static magnetic field, using more P_{NMR} has no further effect on the shift-profile maximum. In Figure 3 the general saturation behaviour of the maximum magnitude of the shift-profiles, as a function of P_{NMR}, is shown. This figure is used later-on for extrapolation to $P_{\mathrm{NMR}} \to \infty$.

3.3 Simulation of shift-profile

For the simulation we started from a system with a homogeneous magnetic susceptibility. A constant separation $d_{\mathrm{PP}} = N^{-1/3}$ is assumed between the ^{31}P atoms. The wave function of each electron is described as hydrogen-like function, centered at the P-atom:

$$| \psi(r) |^2 = A \exp\left\{-\frac{2r}{a_B}\right\} \qquad (2)$$

where r is the distance to the P-atom, and for the Bohr-radius $a_B = 17$ Å [10] was used. From the point of view of the electron spins there are different groups – or shells – of Si-nuclear spins. Each shell i is characterized by the distance r_{ij} to the nearest P-atom j and therefore to the

center of the nearest electron wave function. The hyperfine field for the electron spin j caused by the nuclear spins of group i is given by:

$$\Delta B^{ij} = \frac{8\pi}{3}\hbar\gamma_{\mathrm{Si}}\, I_0(1 - sV_{\mathrm{Si}}) \mid \psi_j(r_{ij}) \mid^2 n_i P_{\mathrm{Si}} \qquad (3)$$

with:

- γ_{Si} is the gyromagnetic ratio of the Si-nuclear spins
- $\langle I_z \rangle = I_0(1 - sV)$: I_0 is the average nuclear spin polarization $\langle I_z \rangle$ in thermal equilibrium. s is the ESR-saturation factor and V_{Si} is the enhancement factor for the nuclear spin polarization caused by the Overhauser effect.
- $\mid \psi_j(r_{ij}) \mid^2$ is the electron density at the lattice site of a Si-atom at distance r_{ij}.
- n_i is the number of Si-lattice sites of group i per P-atom.
- P_{Si} is the natural abundance of the Si-atom with nuclear spin (^{29}Si).

The enhancement factor V_{Si} is proportional to the ratio $\gamma_e/\gamma_{\mathrm{Si}}$ (γ_e is the gyromagnetic ratio of the electron spins). The maximum possible enhancement for the ^{29}Si in Si:P is +3305, but it can be reduced by leakage processes [11]. If the isotropic hyperfine interaction is predominating, the leakage is negligible, but if there exist additional relaxation paths for the nuclear spins, the enhancement of the nuclear spin polarization is reduced.

The hyperfine interaction effects also the resonance of the nuclear spins. Since they are subjected to an additional field, caused by the electron spins, their resonance frequency is shifted by:

$$\Delta\nu_i = \nu_0 \left(\frac{8\pi}{3} \frac{\hbar\gamma_e}{B_{Mess}} S_0(1 - s) \sum_j \mid \psi_j(r_{ij}) \mid^2 \right) \qquad (4)$$

$$= \nu_0 \left(\frac{8\pi}{3} \chi_e (1 - s) \sum_j \mid \psi_j(r_{ij}) \mid^2 \right) \qquad (5)$$

where ν_0 is the nuclear spin resonance frequency caused by the nuclear Zeeman interaction. $\langle S_z \rangle = S_0(1 - s)$ is reduced by the ESR-saturation. Theoretically the interaction has to be sumed up over all electrons in the sample. But the electron density decreases exponentially with increasing distance from the nearest P-atom. Therefore the farther the Si-nuclear spins are from the next P-atom, the smaller is the shift of the nuclear resonance frequency. On the other hand, the number of Si-atoms at a given distance increases with increasing distance. In Figure 4 the product of the number of lattice points at distance d and the electron density at this radius is shown *versus* the distance d. The hyperfine field of the Si-nuclear spins at lattice points farther than 80 Å is negligible. Thus, for the first simulations of the shift profile only Si-nuclear spins within a radius of 80 Å around a P-atom have been taken into account. For each shell of Si-nuclear spins i a Gaussian function f_i with amplitude ΔB_i, center at $\Delta\nu_i$ and a width $\Delta = 0.02$ au was used. Using equations (2–5), we

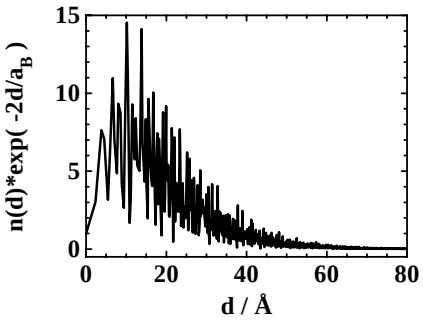

Fig. 4. Product of the decreasing exponential wave function and the number of ^{29}Si nuclei at the distance d of the P-atom *versus* d.

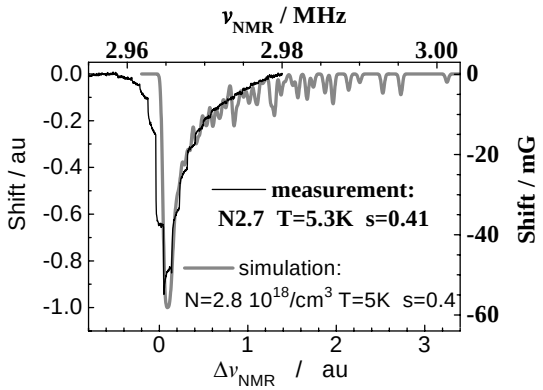

Fig. 5. Comparison of a simulated profile (grey curve, left and lower scale) and the corresponding measurement (black curve, right and upper scale). All the Si-lattice points within a radius of 80 Å around a P-atom have been taken into account for the simulation.

can express the shift amplitude (y) as function of the RF frequency (x) by:

$$y = \sum_i f_i = \sum_i \Delta B_i \, \exp\left\{ -\ln 2 \frac{(x - \Delta\nu_i)^2}{\Delta^2} \right\}. \qquad (6)$$

Time dependent effects, like different time constants for building up the polarization and diffusion of the polarization built-up, have been neglected for the simulations. In Figure 5 a simulated profile (grey) for $N = 2.8 \times 10^{18}/\mathrm{cm}^3$, $T = 5$ K and $s = 0.4$ is shown in comparison to the profile (black), which was measured at the sample N2.7, $T = 5.3$ K and $s = 0.41$. Although the simulation was made for a simplified model, the agreement between the simulation and the measurement is remarkable. It shows that the extended wing at the high frequency side is caused by the distribution of distances between Si-atoms and the next P-atom. The small spikes in the simulated profile are exagerated by the assumption of a small width $\Delta = 0.02$ au of the individual lines, combined with the approximation of a homogeneous magnetic susceptibility and a constant distance d_{PP} between the P-atoms. In the real system the P-atoms are statistically distributed [12] in the sample, and for close P-P neighbour distances (and at least below a certain next neighbour distance) there exist correlations between the electrons. So the susceptibility is

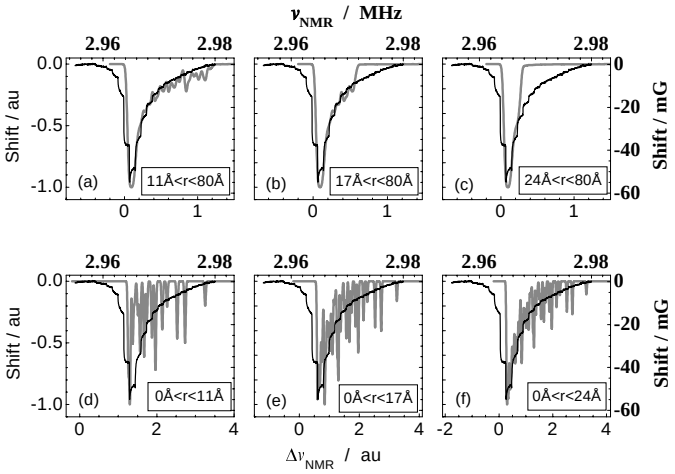

Fig. 6. Comparison of the measurement (black) at N2.7 at 5.3 K and $s = 0.41$ with simulated profiles (grey). At (d–f) only the Si-nuclear spins within a sphere with the given radius have been taken into account. For the calculation of the profiles in (a–c) the Si-nuclear spins within the sphere considered for (d–f) have been neglected. The axis at the right side and at the top are for the measurements. The axis on the left and bottom belong to the simulations and the a.u.s were adjusted accordingly.

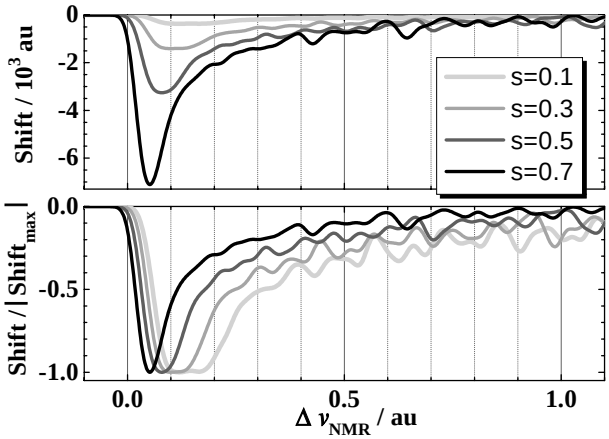

Fig. 7. Change of the simulated profiles with increasing ESR-saturation. The basis profile is the same as in Figure 5. The lower part shows the profiles normalized to the extremum.

not expected to be homogeneous in the sample, and in reality the electron densities cannot be simply summed up, like it was made for the current simulation.

To demonstrate the influence of the coordination sphere, within which the Si-nuclear spins are taken into account, specific simulations have been performed. In Figure 6 the measured profile (black) is the same in all diagrams and identical with that in Figure 5. The simulations are again given as the grey curves. In the lower part the influence only of all Si-nuclear spins within a sphere with smaller radius than $r_{\max} < 80$ Å has been taken into account. For the simulated profiles of Figure 6a–c all Si-lattice points within an outer shell ($r_{\min} < r < 80$ Å) have been taken into account. The diagrams demonstrate clearly, that the nearer the Si-nuclear spins are to the next P-atom and therefore to the center of the electron wave function, the larger is the shift of the nuclear resonance frequency. Figure 6d–f shows that, at least up to distances of about 20 Å, all Si-lattice points have to be taken into account to describe the characteristic shape of the high frequency wing of the profiles. A situation like in Figure 6a would only be realized under the condition that the Si-nuclear spins next to the P-atom loose their polarization by a leakage process that is faster than the characteristic time for the build up of enhanced polarization. Since the hyperfine interaction with the Si-nuclear spins at larger distance is small, it takes more time to build up an enhanced polarization. Thus, it is expected that during the time used for the measurement, it is not possible to polarize all distant Si-nuclear spins. Therefore, if – in contrast to the simulation in Figure 5 – only part of the ^{29}Si nuclei around a P-site contribute, then the situation simulated in Figure 6f is more realistic than that simulated in 6a.

3.4 Influence of the ESR saturation

The ESR-saturation has two different effects on the electron and the nuclear spin system. *Via* the Overhauser effect the nuclear spin polarization is enhanced and therefore the Overhauser shift increases with increasing ESR-saturation (Eq. (3)). On the other hand, saturation of the electron spin system reduces the difference between the occupation numbers of the two electron spin energy levels. This results in a decreasing average electron spin polarization $\langle S_z \rangle$ and therefore decreasing hyperfine field for the nuclear spins: The shift of the nuclear resonance frequency with respect to the bare Zeeman frequency decreases with increasing ESR-saturation (Eq. (4)). Figure 7 shows the effect of the ESR-saturation on the simulated profiles. The diagram at the top clearly demonstrates the increasing ESR-line shift with increasing ESR-saturation. For the diagram at the bottom of Figure 7 the same profiles are shown but this time normalized to the shift extremum. Here the shift of the nuclear resonance frequency $\Delta\nu_{\rm NMR}$ of the extremum to smaller values caused by the reduced hyperfine field for the nuclear spins can be clearly observed.

The results of the measurement for samples N2.7, N3.55 and N5.1.3 are shown in Figure 8 and Figure 9. In Figure 8 again the upper part of the figure shows the profiles with absolute values of the shift. The increase of the shift height with increasing saturation can be clearly observed. At the bottom the corresponding diagram is shown with normalized heights. In spite of the extra structure caused by the 1 kHz steps, it can be observed that the profiles shift to smaller frequencies with increasing ESR-saturation. The reduction of the width of the profiles with increasing ESR-saturation seems to be more significant for the simulations than for the measured profiles, however. The profiles of the samples N3.55 and N5.1.3 (Fig. 9) show the same behaviour as that of N2.7. In this figure the diagrams with the normalized values are shown on the right side.

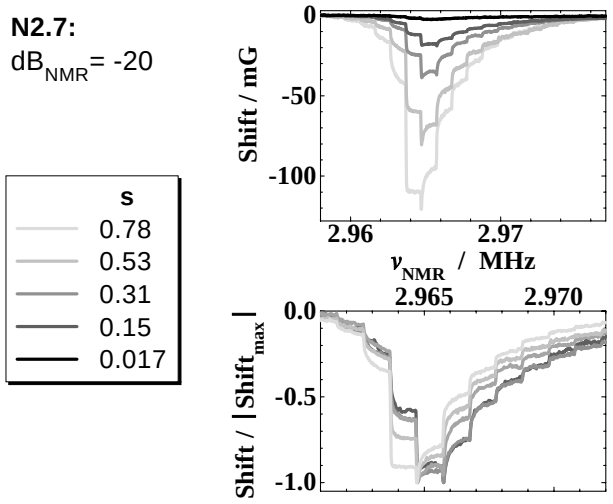

Fig. 8. The measured profiles of N2.7 at 5 K for different ESR-saturations. The figure at the bottom shows the profiles normalized to the extremum.

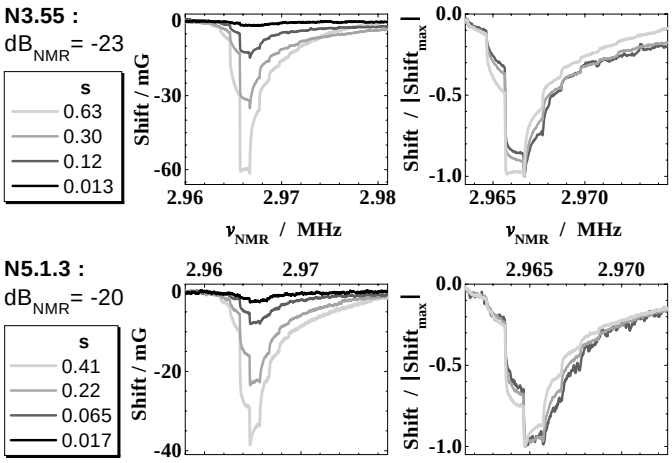

Fig. 9. The measured profiles of N3.55 and N5.1.3 at 5 K for different ESR-saturations. The diagrams at the right side show the profiles normalized to the extremum.

3.5 Influence of the temperature

The average nuclear spin orientation at thermal equilibrium is described by the Curie-law and therefore $I_0 \propto 1/T$. Since the Overhauser shift is proportional to I_0 (Eq. (3)) the height of the shift-profiles is expected to decrease with increasing temperature. Figure 10 shows the simulated profiles for $s = 0$ and $T = 5$, 8 and 11 K. The Curie-like behaviour of I_0 is reflected by the height of the profiles. Figure 11 shows for samples with four different P-concentrations, the measured profiles at different temperatures. The profiles of samples N2.7 and N3.55 follow the Curie-law in the accuracy of the measurement. On the other hand the heights of the profiles of the samples N5.1.3 and N7.3.3 do not increase as much with decreasing temperature, as would be expected by the Curie-law.

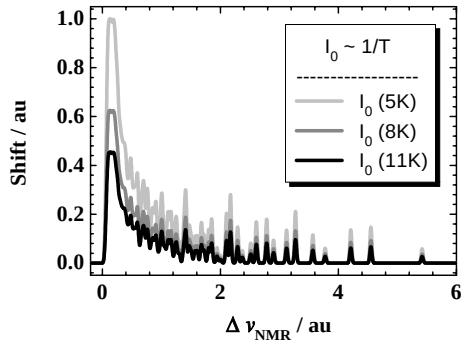

Fig. 10. Change of the simulated profiles for $s = 0.0$ with increasing temperature. The basis profile is the same as in Figure 5.

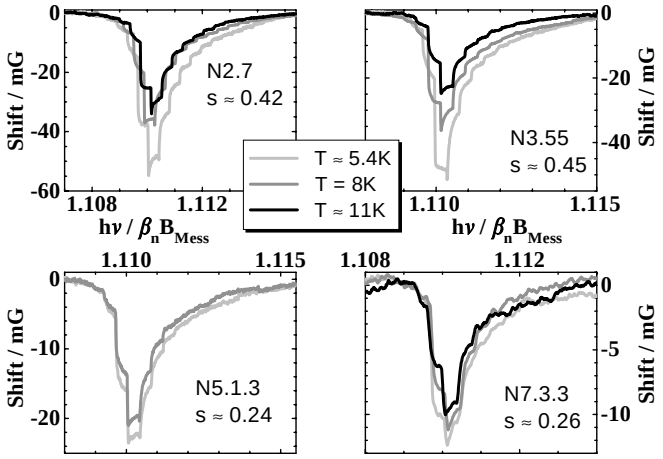

Fig. 11. The measured profiles of N2.7, N3.55, N5.1.3 and N7.3.3 at 5, 8 and 11 K.

4 Time dependence

The Overhauser shift profiles, measured for step-like increasing NMR frequency (see Fig. 1), do not show a step-like shape. Instead they reflect the time dependence of building up or destroying the nuclear spin polarization. Destroying the polarization of the nuclear spins in resonance is a very fast process. During the same time interval the polarization, which was destroyed at lower frequencies is build up again. This process is quite slow (see Sect. 4.2). Since the polarization is destroyed in small spectral and spatial regions, nuclear spin polarization gradients are created by NMR irradiation and result in nuclear spin diffusion. The diffusion is expected to be not very fast, because only 4.7% of the Si-atoms have a nuclear spin. The nuclear spin diffusion will also be hindered with decreasing distance to the nearest P-atom and therefore increasing hyperfine coupling constant and electron spin dipolar field. The different curvature of the Overhauser shift steps at lower and higher NMR frequencies than the extremum of the profile (Fig. 11) can be explained within this framework of time dependent processes and the different shift amplitudes at the next lower and higher NMR-frequency of each step. The time dependence can be characterized in more detail.

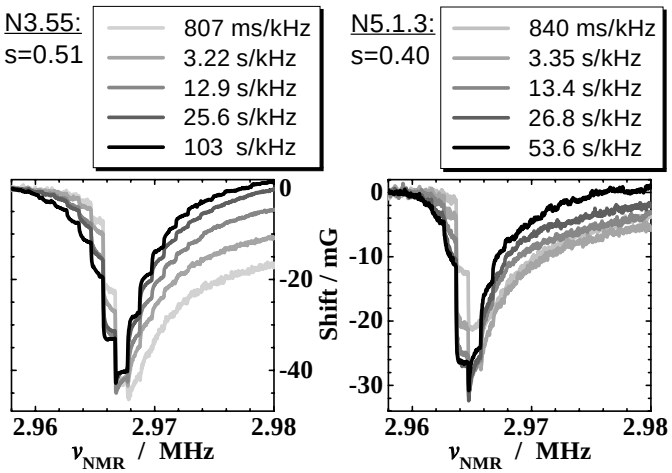

Fig. 12. Change of the profiles with increasing sweep velocity (recorded for increasing frequency).

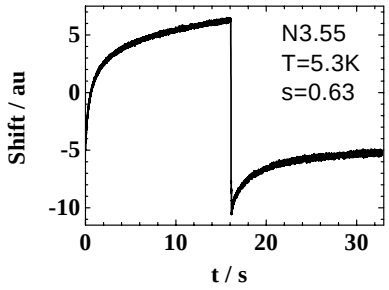

Fig. 13. Measurement of the time dependence of the increase and decrease of the nuclear spin polarization. At $t = 0$ the RF-power is turned off, and after about 16s the power is turned on again.

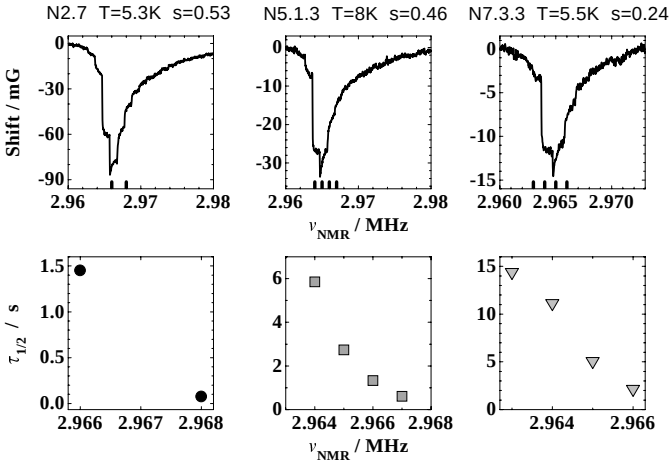

Fig. 14. Characteristic time constant for building-up the Si-nuclear spin polarization for N2.7, N5.1.3 and N7.3.3 *versus* the radio-frequency used previously to destroy the nuclear spin polarization. At the top of each of these figures the relevant profile is shown.

4.1 Time dependence of the profiles

The asymmetry of the Overhauser shift-profiles is related to the distribution of Si-P-atom distances. A distribution of hyperfine interaction results also in a distribution of time constants for building-up the enhanced nuclear polarization by the Overhauser effect. Figure 12 shows profiles of the samples N3.55 and N5.1.3 which have been measured with different frequency sweep velocities. At higher velocity the high frequency wing does not reach the zero line within the sweep time anymore. This means, the sweep time does not suffice to build up the nuclear spin polarization again, which was destroyed at lower frequencies, when the nuclear spins were in resonance. With slower sweep rates the amplitude comes more and more back to the zero line. The effect seems to be more significant for sample N3.55, with smaller P-concentration than for the sample N5.1.3. Except for the results shown in Figure 12, the Overhauser shift profiles of Si-nuclear spins have been measured with slow sweep velocities equivalent to 25.6–26.8 s/kHz.

4.2 Measurement of the time constant

To measure the time constant of the nuclear spin polarization, the ESR-amplitude at constant static magnetic field, P_{ESR} and fixed RF-frequency, was detected time dependently while $P_{\rm NMR}$ was turned on and off in a certain time difference (Fig. 13). Starting with RF on, $P_{\rm NMR}$ destroyed all the nuclear polarization possible at the chosen RF-frequency. At $t = 0$ $P_{\rm NMR}$ was turned off and the detection of the ESR-line shift signal started. The nuclear spin polarization is built up again and therefore the signal increases. After a certain time (16s in Fig. 13) $P_{\rm NMR}$ was turned on again. The polarization of the nuclei at resonance is destroyed immediately and the signal drops steeply. The later slight increase (in Fig. 13) after turning on $P_{\rm NMR}$ again cannot be explained by the Fermi contact interaction of the ^{29}Si spins that are exactly at resonance, but gives a hint, that other interactions influence also the nuclear spin systems.

To determine the time constants for building-up the polarization exponential functions have been fitted to the part of the curves between $t = 0$ and turning on the $P_{\rm NMR}$ again. As expected it turned out that the curve was not monoexponential. For a sample with $N = 3 \times 10^{18}/\mathrm{cm}^3$ this had been reported before [8]. Time dependent measurements have been performed here at different P-concentrations. For N2.7 the curve was fitted with 3 different time constants and with increasing P-concentration less exponential functions were needed. At the highest P-concentration surveyed in this work ($N = 7.3 \times 10^{18}/\mathrm{cm}^3$) one exponential function was sufficient in the accuracy of the measurement. For comparison of the results of different samples and different frequencies the time at which half of the amplitude has been reached again is given in Figures 14 and 15. Figure 14 shows the time constants at different frequencies of N2.7, N5.1.3 and N7.3.3. At the top the corresponding profiles are shown. To have sufficient signal to noise ratio the time dependent measurement had to be performed at frequencies in the vicinity of the shift-peak. Independent of P-concentration the time constant

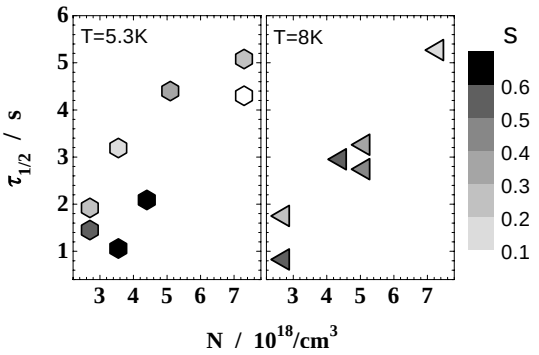

Fig. 15. Time constant at the shift-peak frequency for building-up the nuclear spin polarization *versus* the P-concentration. The results of N7.3 at 5.3 K belong each to one of the two different samples surveyed at this P-concentration.

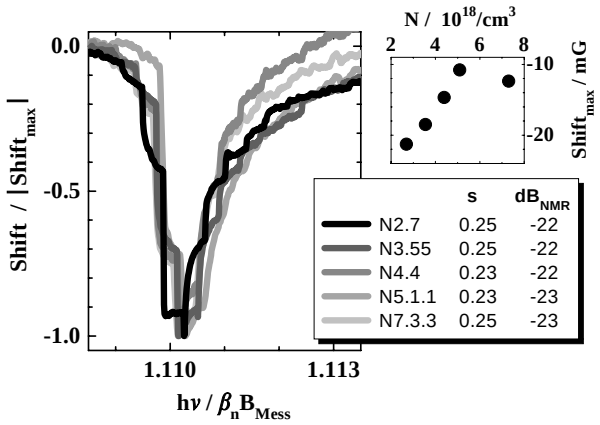

Fig. 16. Si-Overhauser shift-profiles, measured for samples with different P-concentrations at 8 K. The profiles are normalized to the extrema. The heights are shown in the small figure above the legend.

decreases with increasing NMR-frequency within the profile. For a sample with $N = 2.5 \times 10^{18}/\mathrm{cm}^3$ this behaviour was already observed by Jérome *et al.* [5]. This confirms the argument that the shape of the profiles is caused by the distribution of the hyperfine interaction experienced by the Si-nuclear spins. Figure 15 shows the time constants for $T = 5.3$ K and 8 K, measured at the peak frequency, in dependence on the P-concentration. For some samples the time constants are given for different degrees of ESR-saturation and it seems that they become shorter at higher degree of ESR-saturation. As shown in Section 3.4 of this paper, the profiles are narrowed with increasing ESR-saturation factor, because the shift of the nuclear frequency is reduced. From the frequency dependent measurement (Fig. 14) it is known, that the Si-nuclear spins at higher frequencies have shorter polarization times. Because the ^{29}Si resonance frequency of the high frequency wing moves with increasing ESR-saturation towards the peak of the shift-profile, the resulting time constant at the peak becomes shorter. The results at $T = 5.3$ K and $N = 7.3 \times 10^{18}/\mathrm{cm}^3$ (Fig. 15) are obtained for two different samples. In summary, in spite of the somewhat different ESR-saturation factors it can be concluded, that the time constants for dynamic nuclear polarization at the shift-profile extremum become larger with increasing P-concentration. Furthermore at least between 5.3 K and 8 K the time-constant does not change within the accuracy of the measurement.

5 Influence of the P-concentration

Figure 16 shows shift-profiles for the five examined P-concentrations. In the large diagram the profiles are normalized to the peak value for easier comparison of the shapes: The shape of the Si Overhauser shift profiles does not change with increasing P-concentration within the accuracy of the measurement. This indicates that the fundamental form of the wave function, and especially the exponential decay of the electron density distribution, does not change significantly in the surveyed P-concentration range. In contrast, the measurements of the susceptibility have shown a decreasing total susceptibility with increasing P-concentration in the observed range [13–15]. A decreasing local susceptibility would reduce the shift of the nuclear resonance frequency by the hyperfine interaction. Then the profiles would narrow and the extremum could shift to smaller frequencies with decreasing susceptibility. However, within the accuracy of the measurement this behaviour is not observed. This confirms that the principal shape of the Overhauser shift-profiles is dominated by the distribution of Si-P-atom distances. Since the Overhauser shift is the shift of the ESR-line of electron spins with a minimum of exchange interaction, the observed behaviour is related mostly to these electrons and their direct environment.

In the small diagram at the top of the legend the peak values of the shift-profiles are shown (Fig. 16). Although the shape of the profiles does not change, the height decreases by a factor 2 with increasing P-concentration.

6 Analysis of the heights of the shift-profiles

In order to derive a shift-related quantity which is independent of P_{NMR}, the shift-profiles at different P_{NMR} have been measured and extrapolated to $P_{\mathrm{NMR}} \to \infty$ (Fig. 3), to get the shift maximum at the surveyed ESR-saturation factor. For the simulations it was supposed, that only the polarization at the given nuclear spin resonance frequency was thus destroyed completely.

6.1 Results of the simulations

In order to check the influence of individual parameters on the shift value in the shift extremum, dedicated simulations have been performed and analysed. Figure 17 shows the extremal heights of the simulated profiles *versus* ESR-saturation factor for different varied parameters. The curves are all non-linear, since the height increases due to

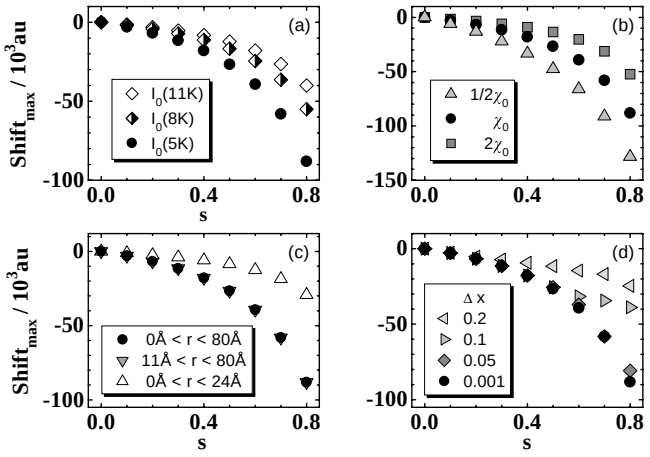

Fig. 17. Height of the extremum of the simulated profiles *versus* the ESR-saturation factor. (a), for different temperatures, (b), for different susceptibilities, (c), for different spatial ranges, within which the Si-nuclear spins have been taken into account and (d), for different resolutions of the frequency axis of the profiles.

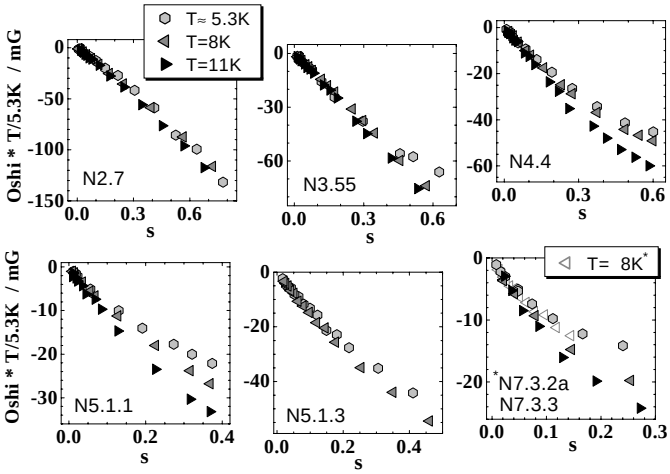

Fig. 18. Height of the extremum of the shift-profiles extrapolated to RF-power $\rightarrow \infty$ *versus* the ESR saturation factor for each P-concentration and for different temperatures. To check the influence of the Curie law of the average nuclear spin polarization the values have been converted to about 5.3 K.

the increasing nuclear spin polarization and in addition, due to the narrowing of the profile (Sect. 3.4).

As described in Section 3.5, the average nuclear spin polarization at thermal equilibrium is proportional to $1/T$. Therefore the extremal shift in Figure 17a decreases with increasing temperature. In Figure 17b the influence of the susceptibility is shown. An increasing local susceptibility causes a larger frequency shift of the nuclear spins and broadened shift-profiles. As a result the extremal height decreases with increasing susceptibility as long as ESR-saturation is $s < 1$. At small saturation the slope of the amplitude *versus* ESR-saturation factors also decreases with increasing susceptibility.

For the shift peak heights, it does not make a big difference ($s < 0.8$), whether all Si-nuclear spins within a sphere with radius 80 Å are taken into account or whether the Si-nuclear spins next to the P-atoms are neglected (Fig. 17c). The reason is that the resonance frequency of the Si-nuclear spins nearest to the P-atom have a large shift $\Delta\nu_{\mathrm{NMR}}$ and they contribute to the extremum only at very high ESR-saturation factor s. The number of Si-nuclear spins at large spatial distance to the nearest P-atom is very large and their resonance frequencies are very close together. Thus, the extremal height of the profile caused by the Si-nuclear spins with separation 0 Å $< r <$ 24 Å from the P-atom is considerably smaller than if all Si-nuclear spins with $r <$ 80 Å have been taken into account (Fig. 17c). Since the resonance frequency for those Si-nuclear spins with $r <$ 24 Å experiences quite a large shift by the hyperfine interaction, but the whole profile is shifted to smaller frequencies already at small ESR-saturation, the corresponding curve of the external height in Figure 17c is more linear for small s than the others.

Since the RF-frequency was swept in steps of $\geq$1 kHz, it was also interesting to analyse which influence the resolution of the frequency has to the change of the height in the extremum. These results are shown in Figure 17d. The simulated profiles shown in this paper have been calculated with a resolution of $\Delta x = 0.001$. If one estimates the corresponding resolution of the measurement by the comparison to the simulated profiles at Figure 6, one derives a resolution of $\Delta x \approx 0.08$ for Figure 6a and $\Delta x \approx 0.2$ for Figure 6f. The curves in Figure 17d show that if the frequency-resolution is reduced, the s dependence approaches linearity, since it is very unlikely to hit the actual extremum of the profile.

6.2 Results of the measurements

Figure 18 shows the heights of the shift-profile extrema extrapolated to $P_{\mathrm{NMR}} \rightarrow \infty$ (Oshi). Under the condition of no Si-nuclear spin diffusion and a perfect resolution of the frequency axis, this would be the extremum of the profiles, if at every NMR-frequency only the corresponding nuclear spin polarization were destroyed totally. It can be generally noticed, that the curves are closer to linearity than most of the results of the simulations. The simulations have shown, that this can be caused by the fact, that the profiles are dominated by the Si-nuclear spins nearby the P-atoms (Fig. 17c) and by the non-negligible 1kHz-steps of the RF-frequency (Fig. 17d). For $N = 7.3 \times 10^{18}/\mathrm{cm}^3$ at about 8 K the results of two different samples are shown. The difference indicates the accuracy of the determination. The difference between the results of N5.1.1 and N5.1.3 is much larger, but the reason for that cannot be explained yet.

The thermal average nuclear spin polarization follows the Curie-law and is therefore proportional to $1/T$. To check this influence on the shift peak height, the values in Figure 18 are multiplied by the temperature of the measurement and divided by the corresponding minimum temperature $T_{min} \approx 5$ K. The results of N2.7 and N3.55 show that the temperature dependence of the profile maximum is clearly dominated by the Curie-law of

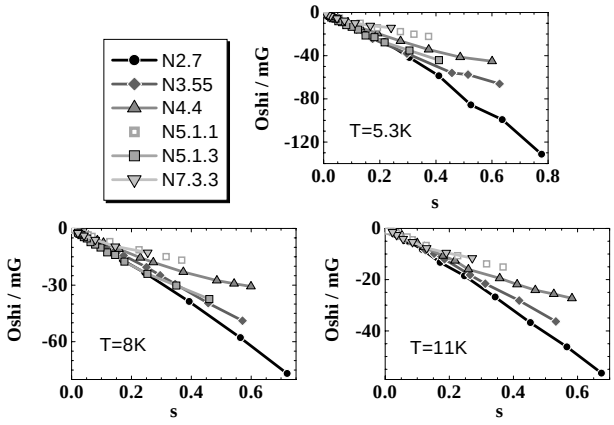

Fig. 19. Extrapolated extremal heights of shift profiles (Fig. 18) as function of ESR-saturation factor at equal temperature and varied P-concentration.

the average nuclear spin polarisation. For the samples with P-concentrations above N_c, the influence of an additional temperature dependent process is observed, *e.g.* the temperature dependence of the leakage process of the enhanced nuclear spin polarisation (Sect. 3.5). The integral shift of the ESR-line due to dynamic nuclear polarization [4] showed comparable temperature dependent behaviour. However the opposite sign of the integral shift indicates the predominance of the P-nuclear spins for an enhanced nuclear spin polarization *via* the Fermi contact interaction.

Figure 19 shows the maximum shift as function of the saturation factor s for equal temperature, so the change with P-concentration can better be followed. Independent on the temperature, the slope of the curves decreases with increasing P-concentration. This confirms the behaviour discussed in Section 5 (Fig. 16). As mentioned before in Section 5, the total susceptibility was reported to decrease with increasing P-concentration. The change of the slope with increasing P-concentration shows the opposite behaviour to the result expected by the simulations for decreasing susceptibility. This confirms again that for the Overhauser shift profiles of the Si-nuclear spins, the total susceptibility of the sample is not the relevant factor. If in contrast the leakage processes become more influential with increasing P-concentration, this would reduce the possible Overhauser enhancement of the nuclear spin polarization and therefore the Overhauser shift.

7 Discussion

The shift of the ^{29}Si nuclear resonance frequency, caused by the hyperfine interaction with the P-centered electron spin decreases with increasing ESR-saturation. For complete saturation, *i.e.* $s = 1$, the average hyperfine field is zero. In the Overhauser shift profiles for different ESR-saturation (Fig. 8 and Fig. 9) the extremum is shifted typically by $\Delta\nu \approx 0.5 - 1$ kHz by the hyperfine interaction. With a Si-nuclear Zeeman resonance frequency of about $\nu_{\rm Si} = 2.964$ MHz this gives a relative shift of $\Delta\nu/\nu_{\rm Si} \approx (1.7 - 3.4) \times 10^{-4}$. Peak-shifts of bulk-Si:P ^{29}Si NMR-spectra in the observed P-concentration range amount to $\Delta\nu/\nu_{\rm Si} \approx (0.4 - 4) \times 10^{-5}$ [16,17], increasing with increasing P-concentration. Only at $N > 2 \times 10^{20}/{\rm cm}^3$ a relative shift of about 1×10^{-4} is observed [16,20]. Also the width at half maximum of the Overhauser shift profiles is by a factor of 3–7 larger than the resonance line of the standard ^{29}Si NMR-spectra in this P-concentration range [16,19–21]. Finally, the longitudinal relaxation time of the Si-nuclear spins, measured with standard NMR-methods for bulk Si:P, is quite different from the time constants determined by the time dependence of the Overhauser shift: At low temperatures the standard NMR method yields time constants between 8−15 min [16,19], while the time constants to build-up the nuclear spin polarization is ≈1−10 s at the Overhauser shift peak frequency (Fig. 15, [8,7]).

All the facts mentioned above prove clearly that in the Overhauser shift measurements only Si-nuclear spins nearby the P-atom and therefore close to the center of the electron wave function are observed. The number of Si-atoms nearby the P-atoms are – relatively – very small in the surveyed P-concentration region. At $N = 2.7 \times 10^{18}/{\rm cm}^3$ only about 8% of all Si-nuclear spins are within a sphere with radius 20 Å around a P-atom and even at $N = 1 \times 10^{19}/{\rm cm}^3$, this portion only amounts to 25%. So at low P-concentration the standard ^{29}Si NMR-signal is dominated by the Si-bulk. With increasing P-concentration, the number of Si-nuclear spins nearby P-atoms increases, and so does their influence on the NMR-spectrum. As a result the relative shift of the standard NMR-line peak increases and the average relaxation time of all Si-nuclear spins decreases, since the relaxation times of the Si-nuclear spins nearby the P-atoms are very short compared to the relaxation time of the main part of Si-nuclear spins. Thus both measuring techniques give complementary information, with the Overhauser shift technique focusing on the really relevant sites of the doped semiconductor.

8 Conclusion

In this paper, measurements and simulations of the ESR-line Overhauser shift profiles caused by the ^{29}Si-nuclear spin polarization in Si:P at the metal-insulator transition are reported and analysed. The results of the peak shift and the relaxation time constants have been compared to results of the standard ^{29}Si NMR measurements reported in the literature. The measurement of the Overhauser shift is confirmed as a method to survey in Si:P the hyperfine interaction of the Si-nuclear spins nearby the P-atoms and therefore close to the center of the electron wave functions. The shape of the Overhauser shift profile is dominated by the distribution of hyperfine interaction strength reflecting the distribution of Si-P-atomic distances. The total susceptibility has no influence on the shape of the shift profile within the accuracy of the measurement. In addition, the functional shape of the profile does not change with increasing P-concentration in the vicinity of N_c, indicating that the exponential envelope function of the electron

wave function is preserved. The height of the extremum of the shift profile decreases with increasing P-concentration, however. A possible explanation could be a reduction in dynamic polarization efficiency by a relative increase of the influence of leakage processes. Since it is not unlikely, that the influence of the leakage processes depends on temperature, the deviation of the T-dependence of the Overhauser shift from the Curie-law, describing average nuclear spin polarization at thermal equilibrium, gives another hint for an increasing leakage rate with increasing P-concentration. A distribution of time constants for dynamic nuclear polarization is observed in all samples, with decreasing time constant for increasing displacement of the NMR frequency with respect to the bare ^{29}Si Zeeman frequency. For the respective extremum of the shift profile, the time constant for building up the nuclear spin polarization by the Overhauser effect increases with increasing P-concentration. These investigations have to be complemented by a corresponding analysis of the ^{31}P Overhauser shift profiles, that will be presented as Part III later on.

We thank H.v. Löhneysen for providing the samples, G. Denninger for discussions and N. Kaplan for a critical reading of the manuscript. This work was financially supported by the Deutsche Forschungsgemeinschaft within the Sonderforschungsbereich 195 (Universität Karlsruhe).

References

1. H. Stupp, M. Hornung, M. Lakner, O. Madel, H.v. Löhneysen, Phys. Rev. Lett. **71**, 2634 (1993).
2. G. Feher, Phys. Rev. **114**, 1219 (1959).
3. A.W. Overhauser, Phys. Rev. **92**, 411 (1953).
4. U. Fasol, E. Dormann, J. Phys. Cond. Matt. **13**, 10065 (2001).
5. D. Jérome, Ch. Ryter, J.M. Winter, Physics **2**, 81 (1965).
6. G. Denninger, *Advances in Solid State Physics*, Vol. 30 (Vieweg, Braunschweig, 1990), p. 113.
7. D. Jérome, Ch. Ryter, H.J. Schulz, J. Friedel, Phil. Mag. B **52**, 404 (1985).
8. V. Dyakonov, G. Denninger, Phys. Rev. B **46**, Rapid Comm., 5008 (1992).
9. U. Fasol, *Messung der Overhauserverschiebung an Si:P im Bereich des Metall-Isolator-Übergangs*, Ph.D. Thesis, Universität Karlsruhe 2001 (Shaker, Aachen, 2001).
10. P.R. Cullis, J.R. Marko, Phys. Rev. B **1**, 632 (1970).
11. A. Abragam, *The Principles of Nuclear Magnetism* (Oxford University Press, London, 1961).
12. T. Trappmann, Ch. Sürgers, H.v. Löhneysen, Europhys. Lett. **38**, 177 (1997).
13. H. Ue, Sh. Maekawa, Phys. Rev. **3**, 4232 (1971).
14. A. Roy, M. Turner, M.P. Sarachik, Phys. Rev. B **37**, 5522 (1988); A. Roy, M.P. Sarachik, Phys. Rev. B **37**, 5531 (1988).
15. H.G. Schlager, *Zur magnetischen Suszeptibilität von phosphordotiertem Silizium am Metall-Isolator-Übergang*, Ph.D. Thesis, Universität Karlsruhe 1996 (Shaker, Aachen, 1997).
16. Sh. Kobayashi, Y. Fukagawa, S. Ikehata, W. Sasaki, J. Phys. Soc. Jpn **45**, 1276 (1978).
17. M.J. Hirsch, D.F. Holcomb, Phys. Rev. B **33**, 2520 (1986).
18. M.J.R. Hoch, U. Thomanschefsky, D.F. Holcomb, Physica B **165&166**, 305 (1990).
19. R.K. Sundfors, D.F. Holcomb, Phys. Rev. **136**, A810 (1964).
20. W. Sasaki, S. Ikehata, Sh. Kobayashi, J. Phys. Soc. Jpn **36**, 1377 (1974).
21. M.A. Paalanen, A.E. Ruckenstein, G.A. Thomas, Phys. Rev. Lett. **54**, 1295 (1985).